Shock-induced termination of reentrant cardiac arrhythmias: Comparing monophasic and biphasic shock protocols

Jean Bragard,[1,a)] Ana Simic,[1] Jorge Elorza,[1] Roman O. Grigoriev,[2] Elizabeth M. Cherry,[3] Robert F. Gilmour, Jr.,[4] Niels F. Otani,[3,5] and Flavio H. Fenton[2]
[1]*Department of Physics & Applied Math., University of Navarra, Pamplona, Spain*
[2]*School of Physics, Georgia Institute of Technology, Atlanta, Georgia 30332, USA*
[3]*School of Mathematical Sciences, Rochester Institute of Technology, Rochester, New York 14623, USA*
[4]*University of Prince Edward Island, Charlottetown C1A 4P3, Canada*
[5]*Department of Biomedical Sciences, Cornell University, Ithaca, New York 14853, USA*

(Received 30 May 2013; accepted 28 October 2013; published online 12 November 2013)

In this article, we compare quantitatively the efficiency of three different protocols commonly used in commercial defibrillators. These are based on monophasic and both symmetric and asymmetric biphasic shocks. A numerical one–dimensional model of cardiac tissue using the bidomain formulation is used in order to test the different protocols. In particular, we performed a total of 4.8 $\times 10^6$ simulations by varying shock waveform, shock energy, initial conditions, and heterogeneity in internal electrical conductivity. Whenever the shock successfully removed the reentrant dynamics in the tissue, we classified the mechanism. The analysis of the numerical data shows that biphasic shocks are significantly more efficient (by about 25%) than the corresponding monophasic ones. We determine that the increase in efficiency of the biphasic shocks can be explained by the higher proportion of newly excited tissue through the mechanism of direct activation. © *2013 AIP Publishing LLC*. [http://dx.doi.org/10.1063/1.4829632]

In the present paper, we show how numerical simulations can be used to understand the efficiency of different defibrillation protocols. Fibrillation is a rapid, irregular electrical activity of the heart. This fatal medical condition is usually treated by the application of an external electric shock to the patient chest through external paddle electrodes. The shape of the electric waveforms that are usually applied are either monophasic or biphasic. This means that in the latter the polarity is switched at some point in the course of the application of the shock. Empirical observations suggest that biphasic shocks are more efficient than monophasic shocks in terminating fibrillation. In this paper, by using a simplified mathematical model of cardiac tissue, which, however, includes a realistic response of the cells to large electric fields, we confirm and explain this experimental observation. The model developed here could be used in subsequent studies in order to design and test more complex waveforms, which could be done systematically because the model is simple and not very computationally costly. The next goal is to find the optimal waveform that reduces the energy needed for defibrillatory shocks. This would be of great benefit for patients undergoing defibrillation by limiting the damage to the heart tissue caused by such a strong electric shock.

I. INTRODUCTION

Cardiac defibrillation is a medical treatment used to terminate ventricular fibrillation or pulseless ventricular tachycardia. An electrical device, via a pair of external thoracic electrodes, delivers a controlled amount of electrical energy to the heart in order to suppress the chaotic cardiac action potentials. The first generation of cardiac defibrillators applied monophasic shocks. Later it was found that switching the polarity of the electrodes during the shock (i.e., a "biphasic" shock) defibrillates the heart more reliably.[1,2] The probability of defibrillation increases, for the same amount of energy applied, for biphasic shocks. Optimal monophasic and biphasic shocks[3] release energies of approximately 200 J and 150 J, respectively. This is a considerable amount of energy, and it is desirable to use less energetic shocks in order to minimize the damage to the cardiac tissue. Indeed, large electric currents irreversibly damage internal tissues.

The efficiency advantage of biphasic shocks over monophasic shocks rests mostly on empirical evidence. Experiments conducted in the late 1980's by Ideker's group provided very important information about defibrillation protocols.[4–6] In these papers, it was shown that biphasic shocks are more efficient than monophasic shocks and that the shape and location of the electrodes (for intra-thoracic shock) also strongly affect the efficiency. In addition, it was shown that some asymmetry in the duration of the biphasic shocks also increases the efficiency. Indeed, shorter second-phase biphasic shocks are more efficient than those with shorter first phase (with the same amount of energy).

At present, there is not yet a full understanding of why biphasic shocks are more efficient than monophasic shocks. From the experimental observations, some tentative explanations were provided by Blanchard and Ideker.[7] These authors identified and studied six potential reasons for the superiority of biphasic shocks versus monophasic shocks. The most convincing one was related to the fact that the first phase of the

a)Electronic mail: jbragard@unav.es

biphasic waveform (hyper-polarization) restores the activity of the sodium channels, which makes defibrillation easier for the second phase (de-polarization). This same argument has been further developed in a theoretical and numerical work by Keener and Lewis.[8] Indeed, in their paper, they showed that biphasic shocks are superior to monophasic shocks because the first phase of the biphasic shock enhances the recovery of sodium inactivation, thereby enabling earlier activation of recovering cells. Keener and Lewis built a one-dimensional cable model of cardiac tissue on a ring to demonstrate the improvement due to biphasic shocks. They also demonstrated the phenomenon in a two-dimensional piece of cardiac tissue. However, the Keener and Lewis paper was not quantitatively accurate because they did not consider separately the intra- and extra-cellular domains of the cardiac tissue. It is now well established that quantitative modeling of defibrillation needs a bidomain formulation that takes into account separately the intra- and extra-cellular domains of the cardiac tissue. Keener and Lewis used the Beeler-Reuter model[9] for transmembrane currents.

Many other theoretical and numerical efforts have been directed towards improving defibrillation protocols.[10–12] The recent paper by Trayanova *et al.*[13] reviews the advances that have been provided by numerical modeling approaches. This paper highlights the importance of the virtual electrode phenomenon (VEP), which describes generation of action potentials in cardiac tissue (generally far from the actual electrodes). Nowadays, VEP is believed to be responsible for the activation of the bulk of the cardiac tissue that is taking place during defibrillation and ultimately for the success or failure of external defibrillation therapy.[14,15]

The present paper follows the line of research developed in the seminal work by Glass and Josephson,[16] who studied the resetting and annihilation of a re-entrant wave on a one-dimensional ring. Comtois and Vinet[17] and Sinha and Christini[18] have extended the study of the re-entry termination by considering multiple stimulating pulses and the inclusion of inhomogeneities along the ring, respectively. In the present paper, we further extend the previous studies by considering the application of very strong stimuli. This is possible only by considering a bidomain model. We also deal with the specific shape of the stimuli and compare the efficiency of the monophasic and biphasic protocols. Finally, in the same vein, recent theoretical works by Krogh-Madsen and Christini[19] and Otani[20] consider the action of up to three successive stimuli in order to eliminate re-entrant activity on a one-dimensional ring of cardiac tissue. In Otani's paper, a one-dimensional ring containing a circulating action potential wave was stimulated by one to three low-energy electric field pulses, modeled as activation of recovered or partially recovered portions of the ring. The wave dynamics itself was modeled through simple action-potential-duration (APD) and conduction-velocity (CV) restitution functions. Otani concluded that there existed a number of combinations of inter-stimulus intervals that could terminate the circulating wave irrespective of the wave's location or dynamical state. This suggested that the corresponding combinations of low-energy electric field shocks, delivered to a fibrillating heart, might extinguish all the circulating waves, terminating fibrillation.

Recent experiments by Fenton *et al.*[21] and Luther *et al.*[22] provide evidence that novel, low-energy shock protocols can improve on existing methods. The new shock protocol employed in these studies was shown to be more effective at low energies if a train of waves, rather than a single waveform, is sent to the fibrillating tissue. The frequency of the wave train is an important parameter in determining the successful outcome of this new defibrillation protocol.

In the present paper, we describe a fast computational method for assessing the effectiveness of any given electric-field-based defibrillation protocol. We use the method to quantitatively compare three different typical defibrillatory shocks: monophasic, symmetric biphasic, and asymmetric biphasic. We also answer the basic question of why biphasic shocks are more efficient than monophasic shocks.

The paper is organized as follows. In Sec. II, we present the model and the dynamics it generates. The response of the cardiac tissue to a strong electric field is discussed in detail and different types of mechanisms associated to the elimination of reentrant dynamics are observed and described in the present model. In Sec. III, we analyze the outcome of a large number of simulations that we have performed for different distributions of heterogeneities and many different initial states of the system. This allows us to perform meaningful statistical analysis in order to rank the three defibrillation protocols. We conclude by proposing further directions of research relevant for anti-arrhythmia therapies.

II. MODEL AND NUMERICAL SIMULATIONS

In this section, we will introduce the model that has been used in this study. As we are interested in a simple model that is not computationally expensive, we turn to a one-dimensional model of cardiac tissue on an annular ring as sketched in Fig. 1.

A. The model

We consider the simplest geometry that sustains a propagating action potential and which has been used extensively in the studies of arrhythmic behaviors—a one-dimensional ring of cardiac tissue, shown schematically in Fig. 1. In a typical simulation, an action potential is initialized, which then propagates around the ring. The shock is modeled as the application of a strong current through the two diametrically opposed electrodes on the ring. This shock can result in the

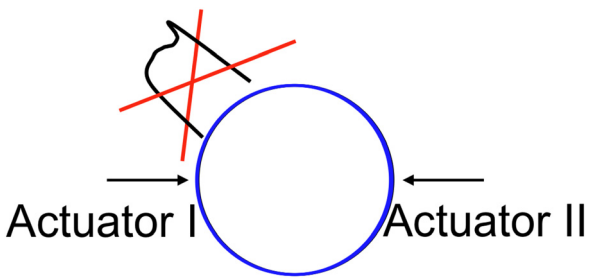

FIG. 1. Schematic of the annular ring of cardiac tissue. Two diametrically opposed actuating electrodes are connected to the extra-cellular domain (shown by the two arrows) and can inject or subtract electrical charges during defibrillatory shocks. A traveling action potential is also shown.

complete removal of any pre-existing wave inside the ring (this is schematically represented by the cross on top of the action potential in Fig. 1). The outcome (success or failure) of the shock is decided by the following simple criterion. If all wave propagation is removed one second after the end of the shock, then the shock is considered successful. If some wave activity is still persistent after one second, then the shock is classified as unsuccessful.

Let us introduce the mathematical equations of the model and then we will proceed to their description.

The model employed here is an extension of the well-known Beeler-Reuter equations[9,23,24] describing the electrical activity of cardiac myocytes. The membrane potential V_m (units mV) is calculated by solving:

$$\frac{\partial V_m}{\partial t} = -\frac{I_{BR} + I_{ep} + I_{fu}}{C_m} + \nabla \cdot (D_g \cdot \nabla V_m) + \nabla \cdot (D_g \cdot \nabla \varphi_e), \tag{1}$$

where C_m is the capacitance per surface area of the myocyte membrane ($\approx 1\,\mu\mathrm{F\,cm^{-2}}$) and where D_g denotes the intra-cellular diffusion of the electrical potential. The electric extra-cellular potential φ_e is obtained by solving the Poisson equation:

$$\nabla \cdot [(D_e + D_g) \cdot \nabla \varphi_e] = -\nabla \cdot (D_g \cdot \nabla V_m) - \frac{I_{ext}}{\beta C_m}, \tag{2}$$

where I_{ext} is the extra-cellular excitation current, β is the myocyte surface-to-volume ratio and here we take $\beta = 1400\,\mathrm{cm^{-1}}$ and D_e denotes the extra-cellular diffusion of the electrical potential, here we take $D_e = D_g = 1.5\,10^{-3}\,\mathrm{cm^2\,ms^{-1}}$. In Eq. (1), the membrane current I_{BR} (units $\mu\mathrm{A\ cm^{-2}}$) is decomposed into four contributions:

$$I_{BR} = I_K + I_x + I_{Na} + I_s, \tag{3}$$

where I_K (sometimes denoted by I_{K1}) is the time-independent potassium outward current, I_x is the time-activated delayed rectifier potassium outward current, I_{Na} is the fast sodium inward current and I_s is the slow calcium inward current. In the present paper, we take the same values for the parameters as in the Courtemanche paper.[23] In particular, we set the value of $\sigma = 0.7$ for the modification of the calcium inactivation gate f, while the calcium conductance is set to $g_s = 0.07\,\mathrm{mS/cm^2}$.

I_{ep} is the current associated with the electroporation phenomenon. Indeed, when the strength of the applied electric field exceeds a few V/cm, reversible pores are created in the myocyte membrane that allow for ion flow across the membrane. As a result, the membrane potential V_m saturates and does not reach unphysiological values for either depolarization or hyperpolarization. This mechanism of electroporation protects the membrane of the myocyte and avoids its breakdown (or lysis). A simple description of the electroporation current was given by De Bruin and Krassowska:[25]

$$I_{ep} = g_p(V_m) N V_m, \tag{4}$$

$$\frac{dN}{dt} = \alpha \exp(\beta V_m^2)\left[1 - \frac{N}{N_0}\exp(-q\beta V_m^2)\right]. \tag{5}$$

Here, we used their model with the original parameters. Note that I_{ep} is only included to Eq. (1) if $V_m > 180\,\mathrm{mV}$ or $V_m < -150\,\mathrm{mV}$.

I_{fu} is an additional current that is needed to account for the possible anode break stimulation of the tissue. We adopt the model described by Ranjan *et al.*[26] to model this effect. Note that the I_K current was also modified according to Ranjan's model. Therefore, the time-dependent block of the rectifier, I_K, at hyperpolarized potentials decreases the membrane conductance and thereby potentiates the ability of I_{fu} to depolarize the cell on the break of an anodal pulse.

Let us comment briefly on the numerical techniques used in this paper. The system size (ring length) is fixed throughout the paper at $L = 6.7\,\mathrm{cm}$ and the spatial discretization is set to $dx = 0.025\,\mathrm{cm}$. The time integration of Eq. (1) is performed with a simple forward Euler scheme. The time step is set to $dt = 0.001\,\mathrm{ms}$ during the shock and for the subsequent 10 ms and then the time step is changed back to $dt = 0.01\,\mathrm{ms}$ for the rest of the simulation. The solution of Eq. (2) for the extracellular potential φ_e is more computationally demanding than Eq. (1). The integration of Eq. (2) is performed by using the generalized minimal residual method (GMRES), which is an iterative Krylov method.[27] Here, we have used the implementation that is freely available from the PETSc open source website.[28] We have selected the additive Schwarz (*asm*) preconditionner for the Poisson solver after performing some preliminary testing and benchmarking with other preconditioners. The convergence of the iterative method was controlled by the residual norm relative to the norm of the right-hand side.[28] Here, we kept the tolerance at its default value, $rtol = 10^{-5}$. The number of internal iterations of the Poisson solver is usually a few but can go up to a hundred at the beginning and at the end of the defibrillatory shock. Note that all the expressions for the currents are computed by using lookup tables. This allows us to avoid the costly computation of exponential functions and the like.

A third modification (after the inclusions of the I_{ep} and I_{fu} currents) with respect to the plain BR model consists of the inclusion of small-scale spatial fluctuations in the electrical internal conductivity of the cardiac tissue. This modification follows from the works of Fishler[29] and Plank *et al.*[30] Indeed, if the cardiac fiber was strictly homogeneous, the effect of the current injection would be localized to within the $O(\lambda)$ region surrounding the electrodes, where λ is a characteristic length scale of the model defined by

$$\lambda^2 = \frac{G_g\, G_e}{G_m\, \beta\, (G_g + G_e)}, \tag{6}$$

where G_g and G_e stand for the intra-(extra)-cellular electrical conductivities, respectively, and have units of $\mathrm{mS\ cm^{-1}}$; G_m is the membrane conductance and has units of $\mathrm{mS\ cm^{-2}}$. The conductivities are related to the previously defined diffusivities by the following equation:

$$D_g = \frac{G_g}{\beta\, C_m}, \tag{7}$$

and a similar equation holds for defining D_e. By replacing parameter values of the present study in Eq. (6) we find

$\lambda \approx 7.10^{-2}$ cm, which is indeed a typical value. The space constant is small compared with the typical spatial extent of cardiac tissue. As pointed out previously,[29,30] it is the heterogeneity of the cardiac tissue that induces electrical polarization throughout the tissue and makes the shock successful. In the present study, heterogeneity is modeled by adding Gaussian white noise to the internal electrical conductivity:

$$G_g(x_i) = \bar{G}_g(1 + \sigma\,\delta_i), \tag{8}$$

where $\bar{G}_g$ is the average value for the internal conductivity and δ_i is a Gaussian white-noise random variable with unit dispersion and $\sigma = 0.15$ is the parameter controlling the strength of the heterogeneities. Let us emphasize that the choice of the white noise reflects the fact that conductivity heterogeneities in the anatomic structure exist at many spatial scales within the normal myocardium, e.g., cell-to-cell variations in myocyte shape, blood vessels, etc. Some recent findings indicate that in some cases there is a well-defined scaling law for size distribution of the heterogeneities.[22] It would be interesting to incorporate these experimental findings in a future study and to see the influence of the size distribution of heterogeneities on the likelihood of defibrillation.

In the present paper, the ring length is chosen such that the action potential exhibits discordant alternans dynamics,[31] a type of quasi-periodic pattern, as it propagates around the ring.[32] Discordant-alternans states are known to be precursors to cardiac fibrillation.[33]

In Fig. 2, we show the membrane potential V_m as a function of position along the ring (denoted in terms of a phase variable $\phi \in [0, 2\pi)$) and time for a typical simulation run. A circulating action potential (i.e., electrical) wave is first initiated. It exhibits discordant alternans, as evidenced by the varying duration of the action potential as it propagates. Discordant-alternans dynamics is characterized by a quasi-periodic wave propagation along the ring.[33] The frequencies associated with this quasi-periodic dynamics can be easily determined by computing the Fourier spectrum. One finds, with the parameters of our model, that the two frequencies are approximately $f_1 = 5.07$ Hz and $f_2 = 0.33$ Hz. The first frequency is associated with the time it takes for a wave to make a trip around the ring, $T_1 = 197$ ms. The second frequency is associated with the time that it takes for a node (see e.g., the node located at the upper left corner in Fig. 2) to make one revolution around the ring, $T_2 = 3030$ ms.

In Fig. 2, at time $t = 0$, the shock is applied. The shock creates a hyperpolarized region (i.e., low values of V_m) in the vicinity of the anode located at $\phi = \pi/2$, while at location $\phi = 3\pi/2$ one observes a depolarized region (high values of V_m) due to the presence of the cathode. In the particular case shown in Fig. 2, the shock was successful. As the purpose of the paper is to compare the relative efficiency of different defibrillation protocols, let us turn now to the definition of these protocols.

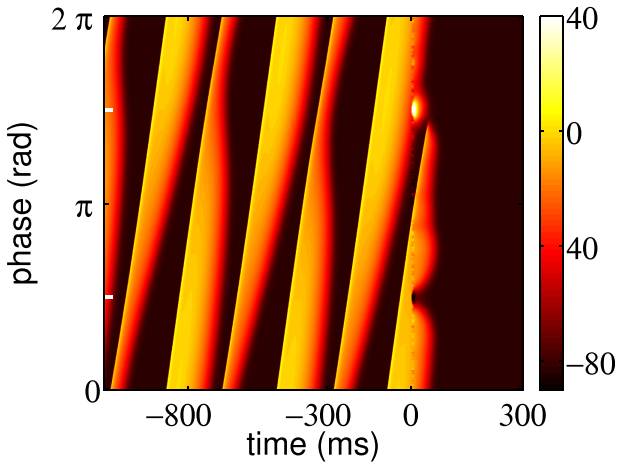

FIG. 2. Space–time plot showing the wave dynamics on the ring. The color scale represents the membrane potential V_m ranging from −90 to +40 mV. Note that the hyperpolarized—(around −136 mV) and depolarized—(around +155 mV) regions are out of scale at time $t = 0$. The undisturbed dynamics ($t < 0$) represents discordant alternans. At $t = 0$ a monophasic shock of 8 ms duration with a corresponding electric field intensity of $E = 2$ V/cm is applied. In this particular case, the shock leads to a suppression of the wave propagation. The two electrodes are located at $\pi/2$ and $3\pi/2$ along the ring (shown by thick white segments in the vertical axis).

B. Comparing three standard defibrillation protocols

The most common protocols used in commercial defibrillators are monophasic and biphasic. Nowadays, most of the new defibrillators are biphasic due to their superior efficiency. An asymmetric biphasic protocol where the first phase is longer than the second phase is currently the method of choice. In Fig. 3, we illustrate graphically the three protocols tested in the present paper. As shown in Fig. 3, we have used step functions for the switching on and off of the shock which is an approximation that simplifies the problem. Indeed, due to physical constraint imposed by the discharge of the capacitors that store the electric charges inside the defibrillators, there is actually a time constant associated with charging and discharging of the capacitors. A more realistic function (exponential relaxation) for the current injection will be considered in a future work.

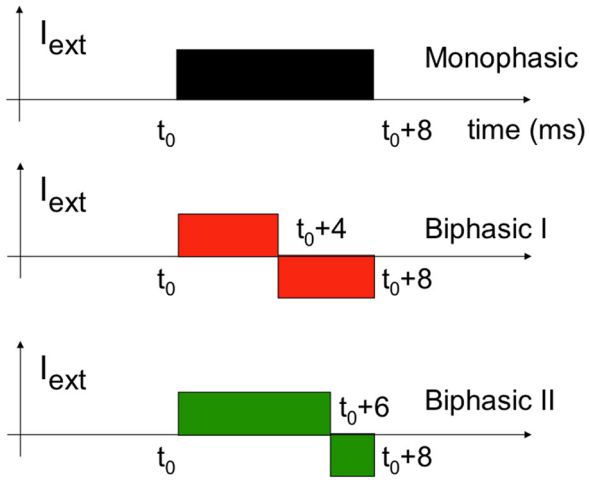

FIG. 3. The three shock waveforms analyzed in this paper: monophasic, biphasic I (symmetric), and biphasic II (asymmetric). I_{ext} is the current injection term that appears in Eq. (2). The currents shown here are the ones that are applied by the electrode that is located at position $\phi = \pi/2$; the currents applied by the other electrode (located at $\phi = 3\pi/2$) have the same magnitude but opposite polarity.

C. Parameters influencing the defibrillation outcome

Before going straight to the simulation results of our model, one can anticipate the important parameters that will influence the defibrillation outcome. Even though we are dealing with a simple 1D model, the number of parameters is large. Let us list the parameters influencing defibrillation.

1) *The shock waveform* (see Fig. 3) is a determining factor for the elimination of reentrant dynamics. The quantification of the influence of this factor is the main motivation behind the present work. By using statistical tools, we will rank these three protocols in term of measured efficiency.
2) *The shock duration*: indeed, one intuitively expects that the longer the shock, the higher the probability to defibrillate. In the medical literature[34] the curve relating the intensity of the shock (associated with a 50% positive outcome) with the shock duration is called the *strength-duration curve*. The construction of such a curve requires a large number of experiments and cannot be obtained directly for humans. The curve is usually inferred from experiments performed with animals. In the present work, we will not study shock duration and the shock duration will be fixed for the rest of the paper at 8 ms, which is a typical value used in commercial defibrillators.
3) *The shock energy* is another parameter influencing defibrillation. Here we will study shocks of increasing energies. More precisely, here we will vary the electric field (units V/cm) associated with the shock from $E = 1$ V/cm to $E = 10$ V/cm. The square of the electric field is directly proportional to the energy.
4) *Shock timing* is another parameter that can influence the outcome. At the time of the application of the shock, we will record ϕ_i and ϕ_b, defined to be locations of the action potential wave front and wave back, respectively. (The wave front and wave back are defined as the points at which the membrane potential crosses a threshold value representing 10% of the maximum value of V_m during depolarization.) As will become clear from the analysis of the results, ϕ_b is an important parameter in determining the outcome of the shock.
5) *Dynamical state at the time of the shock*. The dynamics of the action potential is quasi-periodic (discordant-alternans), so the size of the action potential $\Delta\phi = (\phi_i - \phi_b) \bmod 2\pi$ (measured in terms of the phase difference) is a constantly varying parameter. From the analysis of the simulations (see Sec. III C), we will see that $\Delta\phi$ is also important in determining the defibrillation outcome.
6) *Heterogeneity of the cardiac tissue*. The intensity and to some degree the realization of the noise has an influence on the defibrillation outcome. The higher the noise intensity, the lower the energy needed to defibrillate. Clearly, a high level of heterogeneities in the cardiac tissue is favorable because the heterogeneities create additional polarization sites that help excite more of the tissue. For the rest of the paper, we have fixed the amplitude of heterogeneity at $0.15\,\bar{G}_g$.
7) *The system size* is also a parameter that influences the dynamics and consequently the results of the defibrillation shocks. In the present paper we have fixed the system size at $L = 6.7$ cm, which corresponds to quasi-periodic dynamics of the action potential. By varying the parameters of the membrane model and the system size, one can get different dynamics, e.g., a chaotic dynamics for the action potential propagation on a 1D ring, as explained in the work of Garfinkel and coworkers.[35] Preliminary results obtained for the model of Garfinkel indicate that the results presented in this paper are still valid. We plan to repeat our analysis by using the chaotic model as the starting undisturbed dynamics in a subsequent investigation. As the reader can easily understand, even this simple model on a 1D ring is too rich to be explored in full generality and we have to restrict the focus of the analysis.

D. Mechanisms for elimination of reentrant dynamics

In order to build some intuition of how the shock influences the propagating action potential wave in our model, we compare the results of several qualitatively different simulation runs. Figure 4 illustrates the four different mechanisms that can be indentified. Fig. 4(a) illustrates the first mechanism, which we call Direct Block (DB) where the front is very close to the anode when the shock is initiated and is directly blocked. The DB mechanism is clearly the least common mechanism and is only present at low energy and especially for the monophasic type of protocol. Fig. 4(b) illustrates the second mechanism, which is called Annihilation (An) and which corresponds to the elimination of two (or any even number of) counter-propagating waves that annihilate each other. Note that in Fig. 4 the speed of the waves appears to vary abruptly at $t = 18$ ms. This is because the time scale (horizontal axis) has a nonuniform scale (corresponding to the change in the time step). Fig. 4(c)

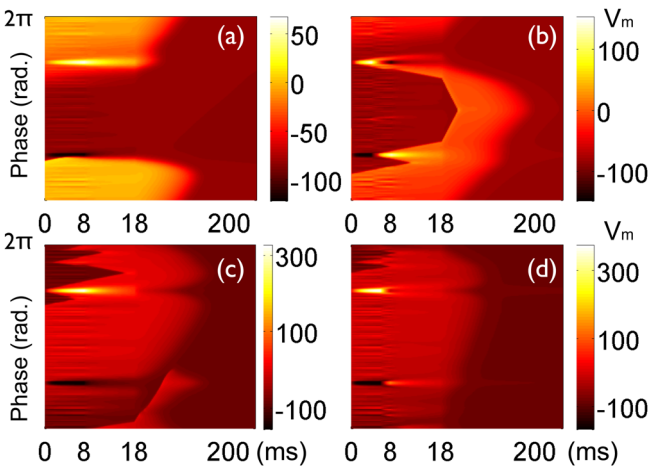

FIG. 4. Color space-time plots of V_m showing the four different mechanisms for reentrant dynamics removal: (a) mechanism of Direct Block (DB) ($E = 1$ V/cm, monophasic); (b) mechanism of Annihilation (An) of two counter-propagating fronts ($E = 3$ V/cm, biphasic I); (c) mechanism of Delayed Block (De) showing that a single wave encounters a refractory region and is finally blocked ($E = 4$ V/cm, monophasic); (d) mechanism of Direct Activation (DA) showing that a large proportion of tissue is excited and then relaxed to the rest state ($E = 6$ V/cm, biphasic II). Note that for all the four plots (a)–(d), the horizontal time scale is not constant. The time resolution is enlarged by one order of magnitude up to 18 ms in order to highlight the effect of the shock. The shock is always initiated at $t = 0$.

illustrates the third identified mechanism that we call Delayed Block (De), which corresponds to a single surviving wave that finally encounters a refractory region and dies out. Fig. 4(d) illustrates the last mechanism, which we call Direct Activation (DA). This mechanism is dominant at high energy (see Sec. III C). It corresponds to a large portion of the tissue being excited by multiple virtual electrodes. The entire ring is then excited, the action potential cannot propagate any longer and eventually the tissue relaxes towards the rest state. The DA mechanism is the defibrillation mechanism that is usually known and referred to in the medical literature. It is also the most robust mechanism in term of the dynamics. Indeed, mechanisms DB, An, and De are probably less present in higher dimensions and more complicated geometries. We do not have enough evidence at this point to generalize those mechanisms to higher-dimensional systems. However, mechanism DA is presumably independent of the dimensionality of the system (1D, 2D, or 3D).

III. MONTE–CARLO SIMULATIONS

In this section, we will test the efficiency of the shock application. In particular we will do an exhaustive survey of the parameters 1, 3, 4, 5, and 6 defined in Sec. II C. We have performed a total of 4.8×10^6 simulations. This number corresponds to the product of the following: 3 protocols (parameter 1 of Sec. II C), 10 values of the electric field ranging from 1 V/cm to 10 V/cm (parameter 3 of Sec. II C), 2000 different initial conditions of the undisturbed dynamics at the shock initiation (parameters 4 and 5 of Sec. II C), and, finally, 80 different random realizations of heterogeneity in the internal conductivity (parameter 6 of Sec. II C).

Indeed, as the dynamics is quasi-periodic (see Fig. 2), one never gets back to the exact same condition if one follows the undisturbed dynamics. Therefore, the 2000 initial conditions consists of a large sample of the dynamics, and consequently a representative sample of the parameter 4 and 5 of Sec. II C. The 2000 initial conditions (IC) were taken as follows: after an initial long transient (several tens of seconds) that we discard, one starts the defibrillation testing. The system evolves freely for a picked uniform random time ranging from 28 to 38 ms, then one saves the full system state variables and proceeds to test the shock outcome of all 3 protocols, the 10 levels of energy and the 80 realizations of the heterogeneity. Once done, the results are saved in a file and one proceeds to pick again a random time ranging from 28 to 38 ms and let the system evolve for this amount of time up to the next IC. This procedure is repeated 2000 times.

A. Automatic classification of the simulation data by artificial neural networks

The next step consists of classifying the results of the numerical simulations. One considers the shock successful if the wave is eliminated during the 1000 ms interval following the end of the shock application, which corresponds approximately to the time it takes the undisturbed wave to complete five rotations around the ring. If the shock was successful, one needs to further classify the reentrant dynamics removal into one of the four mechanisms illustrated in Fig. 4.

Because of the large number of simulations, manual classification would be extremely time consuming. We have therefore performed an automatic classification of reentrant dynamics removal mechanisms using an artificial neural network (ANN).[36] During each simulations, one computes at every millisecond the location and direction of propagation of all the wavefronts present in the ring. At the end of each simulation, one saves a vector of fifty entries that summarizes this information. This vector serves as the input for the ANN. As is typical for ANN, an initial learning phase (or stage) is required before the ANN can be used for automatic classification. Here, we have limited the analysis of the reentrant dynamics removal mechanisms to the values of the electric field corresponding to E = 1, 3, 5, and 7 V/cm (see Fig. 5).

For each level of energy, 1200 data sets (400 of each of the three protocols) were used for the learning phase of the corresponding ANN. In the learning phase, we used cross-validation partition of the training data in order to create several distinct copies of the ANN. Specifically, we have separated the 1200 data sets into 5 partitions each containing 240 data sets for the validation and 960 for the creation of the ANN. In order to increase the accuracy of the classification, we used two types of ANN, one with one hidden layer

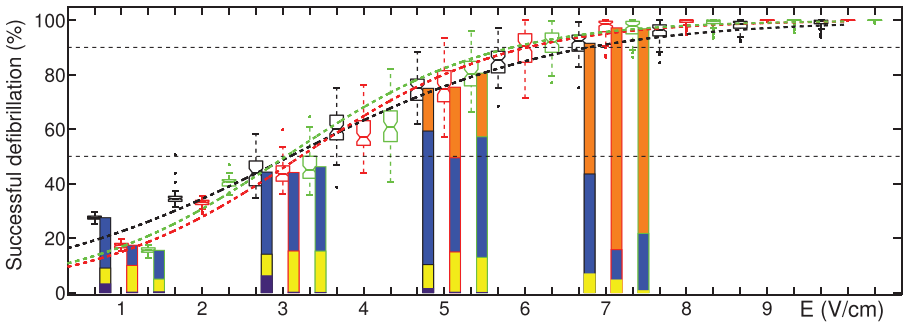

FIG. 5. Fitted logistic curves (see Eq. (9)) for the three different shock protocols: Monophasic (black); Biphasic I (red) and Biphasic II (green). Also depicted are the box plots showing the dispersion in the results due to the heterogeneities in the internal conductivity. In order to avoid overlap of the box plots, we have shifted to the left (by 1/3 V/cm) all the box plots associated with the monophasic protocol (in black) and we have shifted to the right (also by 1/3 V/cm) all the box plots associated with the biphasic II protocol (in green). The box plots associated with the biphasic I protocols (in red) as well as all the logistic curves have not been shifted. The horizontal dashed lines at 50% and 90% are plotted to ease the comparison between the three protocols. The information about the defibrillation mechanisms at work at selected values (E = 1; 3; 5; 7 V/cm) of the energy is also displayed. The color coding is the following: DB (purple); An (yellow); De (blue); DA (orange).

of 20 neurons and one with two hidden layers of 14 neurons. These choices were motivated by comparing the results of automatic classification by various ANN with human analysis of a portion of the complete data set. The results of the classification are summarized in Table I. All the calculations associated with the ANN analysis were performed with the Neural Network Toolbox of Matlab.[37]

Table I allows one to draw some interesting conclusions. At low energy (E = 1 V/cm), quite surprisingly, the monophasic shocks are more efficient than the biphasic shocks. This can be explained by the fact that at low energy the switch in polarity for biphasic protocols leads to a compensation and hinders the shock efficiency. Indeed, the charge delivered during the shock is too weak to restore the activity of the sodium channels and so does not help in the recovery of the excitability of the myocytes. From the values given in Table I, it appears that the DB mechanism is very specific to the monophasic shocks and low energy levels. The classification into different mechanisms is more complicated at energy E = 5 V/cm and E = 7 V/cm. The error in classification that is obtained from the cross-validation procedure and measured by the standard deviations (shown in parentheses in Table I) is larger for higher energies. In order to reduce the uncertainty of the classification, we have doubled the ANNs for high energy values, i.e., 20 ANNs rather than 10 for lower energies. Also, at low energy, it is apparent that the Biphasic II shock is significantly more efficacious than the Biphasic I shock. For weak pulses of duration comparable to the shortest characteristic time scale of the dynamics (associated with the sodium gating), the effect of the electrical perturbation, in the linear approximation, is given by the integral of the perturbation signal, so that the reversal of polarity decreases the response of the tissue. For a very short Biphasic I shock, the effect of the two phases would cancel out completely, while for the Biphasic II shock, the effect of the longer first phase would not be canceled by the shorter second phase, making it more effective. For longer shocks, the cancellation is not complete but, by continuity, this still leaves Biphasic II more efficient than Biphasic I.

At high energy, the biphasic shocks are more efficient than the monophasic shocks. Furthermore, Table I shows that the DA mechanism is prevalent at high energies and for biphasic shocks. Let us recall that this DA mechanism is the most robust one since it is expected to work in any number of spatial dimensions. We think that this is the key for explaining why the biphasic defibrillation shocks are more efficient than the monophasic shocks. The high incidence of the DA mechanism for biphasic shocks coincides with the high proportion of tissue that is excited by the shock through the creation of virtual electrodes.

B. Dose-response curves

In this section, we continue the analysis of the simulation results by concentrating on the outcome of the shock rather than the reentrant dynamics removal mechanism. The traditional way to quantify the efficiency of shocks is through a Dose-Response curve, which reflects the simple fact that the higher the energy in the shock, the higher the probability to defibrillate. As expected, the probability saturates at large energies and at some point it becomes useless to increase further the shock intensity.

Following the standard practice of medical defibrillation studies, one can fit the data for the probability of success p as a function of the applied electric field E with a logistic curve:

$$\log\left(\frac{p}{1-p}\right) = \beta_0 + \beta_1 E. \tag{9}$$

The fitting parameters β_0 and β_1, as well as their respective standard errors, are given in Table II for the three protocols compared here. Let us recall that for each value of the electric field E and for each protocol, we have collected the data representing the outcomes of a total of 160 000 simulations

TABLE I. Classification of the outcomes of reentrant dynamics removal obtained by the ANN analysis for shocks of four different levels of energy. The probability (in percents) and its standard deviation (in parentheses) is given for each outcome.

E (V/cm)	Protocol	Failure	Direct block	Annihilation	Delayed block	Direct activation
1[a]	Monophasic	72.51	$3.16_{(0.08)}$	$5.81_{(0.15)}$	$18.51_{(0.16)}$	0
	Biphasic I	82.64	$0.099_{(0.071)}$	$9.83_{(0.11)}$	$7.42_{(0.12)}$	0
	Biphasic II	84.52	$0.26_{(0.018)}$	$4.67_{(0.083)}$	$10.55_{(0.08)}$	0
3[b]	Monophasic	55.77	$6.13_{(0.25)}$	$7.92_{(0.34)}$	$30.17_{(0.27)}$	0
	Biphasic I	55.92	$0.106_{(0.08)}$	$15.16_{(0.37)}$	$28.82_{(0.38)}$	0
	Biphasic II	53.78	$0.006_{(0.01)}$	$15.17_{(0.67)}$	$31.04_{(0.67)}$	0
5[c]	Monophasic	25.03	$1.45_{(1.91)}$	$8.80_{(0.98)}$	$49.04_{(2.17)}$	$15.68_{(2.32)}$
	Biphasic I	24.60	$0.084_{(0.106)}$	$14.80_{(1.24)}$	$34.58_{(1.51)}$	$25.93_{(1.84)}$
	Biphasic II	19.44	$0.003_{(0.008)}$	$12.88_{(1.18)}$	$44.31_{(1.66)}$	$23.36_{(1.92)}$
7[d]	Monophasic	8.50	0	$6.82_{(1.10)}$	$36.72_{(2.64)}$	$47.96_{(2.78)}$
	Biphasic I	2.795	0	$4.60_{(0.96)}$	$11.17_{(2.08)}$	$81.44_{(2.37)}$
	Biphasic II	3.129	0	$0.67_{(0.21)}$	$21.02_{(1.92)}$	$75.18_{(1.89)}$

[a]Number of ANN used for this energy is 10.
[b]Number of ANN used for this energy is 10.
[c]Number of ANN used for this energy is 20.
[d]Number of ANN used for this energy is 20.

TABLE II. This table gives the confidence intervals (with $\alpha = 0.01$) for the electric fields needed to get 50% (E_{50}) and 90% (E_{90}) of successful reentrant dynamics removal, respectively. The second column gives the fitting parameters of all the simulation data with a logistic curve (see Eq. (9)). The standard error for each of the fitting parameter is also given (small sub-indices in parentheses next to each parameter).

Protocols	Fit parameters	E_{50} (V/cm)	E_{90} (V/cm)
Monophasic	$\beta_0 = -1.835_{(.004)}$	[3.08 – 3.10]	[6.77 – 6.80]
	$\beta_1 = 0.5942_{(.001)}$		
Biphasic I	$\beta_0 = -2.521_{(.005)}$	[3.21 – 3.23]	[6.02 – 6.04]
	$\beta_1 = 0.7826_{(.001)}$		
Biphasic II	$\beta_0 = -2.383_{(.005)}$	[3.03 – 3.05]	[5.83 – 5.85]
	$\beta_1 = 0.7844_{(.001)}$		

(2000 initial conditions times 80 realizations of the tissue heterogeneity). These data form a large sample described by a binomial distribution. Because of the large number of simulations, the standard errors obtained in Table II for the fitting parameters are very small. Also reported in Table II are the computed confidence interval (with $\alpha = 0.01$) of the electric fields corresponding to 50% and 90% of success. One can see that the values for the electric field corresponding to the 50% probability of reentrant dynamics removal (E_{50}) are similar for the three protocols. In contrast, one can clearly rank the values for the electric field corresponding to the 90% probability of reentrant dynamics removal (E_{90}). The biphasic II protocol requires the lowest field strength (and energy) for reentrant dynamics removal with a 90% success rate. We find a decrease of approximately 26% in the energy (proportional to the square of E_{90}) for the biphasic II protocol relative to the monophasic protocol. This is in very close agreement with the values found in the medical literature,[4,5] which cites a decrease in energy of about 25% for biphasic defibrillators with respect to their monophasic counterparts.

The graphical representation of the logistic curves for the three protocols is provided in Fig. 5. Furthermore, this graph also shows the dispersion of the results due to the heterogeneities in the internal conductivity. As mentioned before, we have 80 different realizations for the noise in the conductivity. The results of the 2000 simulations (with different ICs) show significant variation in the probability of successful reentrant dynamics removal. We have used the standard representation of box plots to represent the dispersion associated with the heterogeneity in the internal conductivity. The box plots used here show the median and its corresponding notches for the median dispersion that indicate a 95% probability for the confidence interval of the median. Note that the notches are computed using the underlying assumption of a normal distribution. As shown in Table IV (in the Appendix), this assumption is not always satisfied, especially for high-energy shocks. Note that the outliers are also plotted in Fig. 5 as small dots that lie outside the extension of the whiskers.

As one can see from Fig. 5 and as expected, the dispersion is greater in the central part of the logistic curves. Recall that the variance of a binomial distribution is $Np(1-p)$ and is maximal when $p = 1/2$. For the 50% probability of reentrant dynamics removal, the logistic curves are very close to each other and it is very difficult to decide which protocol is more efficient. On the contrary, if one considers a 90% probability of reentrant dynamics removal, the results clearly indicate that the two biphasic protocols are more efficient than the monophasic protocol. At high energy, biphasic shocks prove to be more efficient because the DA mechanism is dominant there, as shown in Fig. 5.

To conclude this section, we provide a pairwise statistical comparison between the three protocols at each level of the electric field (E ranging from 1 to 10 V/cm). Table III summarizes the findings. As it appears that the distributions of reentrant dynamics removal probability generated by the variation of the heterogeneities are not Gaussian in general (see Table IV in the Appendix), one has to use non-parametric testing for statistical comparison. Here we have used the pairwise Wilcoxon rank sum test for determining whether the medians for the distinct protocols are statistically different. A close look at Table III once again confirms that at the lowest energy (corresponding to $E = 1$ V/cm), the monophasic shocks are the most efficient. For high energies (corresponding to $E > 5$ V/cm), the biphasic shocks are statistically more efficient than the monophasic shocks, while the efficiency of the two biphasic shocks is comparable. However, for E ranging between 2 V/cm and 5 V/cm the biphasic II is clearly more efficient than the biphasic I. One can conclude that at lower energies, but not the lowest, biphasic II shocks combine the positive effects of both monophasic and biphasic shocks and therefore is ultimately the most efficient type of shock.

C. Relation between the dynamics, timing and shock outcome

It is often stated that defibrillation is intrinsically stochastic, and, traditionally, statistical analysis has been the tool of choice for analyzing defibrillation data. Following the tradition, in this section, we are going to use statistical analysis to uncover the relation between the positions of the wave front and back at the moment of the shock application (see Sec. II C) on the outcome of reentrant dynamics removal.

TABLE III. A comparison of the medians of the distribution (corresponding to all the box plots shown in Fig. 5) for the three protocols at different energies. The statistical comparison is realized through a pairwise Wilcoxon rank sum test for equal medians. The comparison is then translated into a Z-score in order to see the significant differences more clearly.

$E_{(V/cm)}$	Mono.	$Z_{(M-BI)}$	B.I	$Z_{(BI-BII)}$	B.II	$Z_{(M-BII)}$
1	27.50	10.92	17.33	8.52	15.50	10.92
2	34.48	6.57	33.10	−10.92	40.65	−9.94
3	43.93	−0.32[a]	43.38	−2.43	45.13	−2.14
4	59.93	2.07	56.93	−2.11	60.78	−0.35
5	75.10	−0.23	74.75	−3.84	80.35	−5.29
6	85.23	−4.76	90.43	−1.64	92.13	−6.94
7	92.50	−8.10	98.53	0.81	97.88	−7.71
8	96.58	−8.92	99.90	1.41	99.78	−7.84
9	98.75	−10.10	100	1.07	100	−8.73
10	99.68	−9.26	100	0.07	100	−8.91

[a]In this table, gray color is used for non-statistically-significant differences at the $\alpha = 0.05$ level (one-sided test).

TABLE IV. The χ^2 goodness-of-fit test of the default null hypothesis that the data are a random sample from a normal distribution with mean and variance estimated from the data. The notation "1" means that the null hypothesis can be rejected at the $\alpha = 0.05$ significance level, while "0" means that the null hypothesis cannot be rejected. The p-values are also given in parentheses.

$E_{(V/cm)}$	Monophasic	Biphasic I	Biphasic II
1	$0_{(0.268)}$[a]	$0_{(0.578)}$	$0_{(0.206)}$
2	$1_{(0)}$	$0_{(0.518)}$	$0_{(0.229)}$
3	$0_{(0.598)}$	$1_{(0.046)}$	$0_{(0.371)}$
4	$0_{(0.9)}$	$0_{(0.091)}$	$0_{(0.554)}$
5	$0_{(0.08)}$	$0_{(0.205)}$	$0_{(0.704)}$
6	$0_{(0.482)}$	$0_{(0.112)}$	$0_{(0.84)}$
7	$1_{(0.027)}$	$1_{(0.002)}$	$0_{(0.08)}$
8	$0_{(0.149)}$	$1_{(0)}$	$1_{(0)}$
9	$1_{(0.003)}$	$1_{(0)}$	$1_{(0)}$
10	$1_{(0)}$	$1_{(0)}$	$1_{(0)}$

[a]As usual, the p value is the probability, under assumption of the null hypothesis, of observing the given statistic or one more extreme. Here (0) means that ($p < 10^{-4}$).

Quite surprisingly, we shall see that, at least in the simple model presented here, the knowledge of these two parameters can be used to reliably predict the shock outcome, especially for low energy. This seems to indicate that the stochastic view of defibrillation is only indicative of our lack of knowledge of fibrillation dynamics. Of course, the one-dimensional model presented here does not capture the full complexity of the real tissue. In a more realistic three-dimensional model, the effect of the shock on the dynamics becomes much more complex.

Our results are summarized in Figs. 6–9. Each figure represents a 2D color histogram showing the probability of defibrillation for the three protocols. We use the same convention for all the graphs: the upper, medium and lower rows are for monophasic, biphasic I, and biphasic II, respectively. The horizontal and vertical axes of each of the subplots represent the values of the action potential duration $\Delta\phi$ (describing the current state) and the location ϕ_b of the wave back on the ring (describing the shock timing). It may seem non-straightforward that we have chosen to use the position of wave back (ϕ_b) rather than the wave front (ϕ_i) as our measure of the shock timing. But previous studies[38–41] have shown that, for cardiac wave propagations, the dynamics is more sensitive to perturbations applied at the wave back rather than the wave front. This is again confirmed in the present study; a careful look at Figs. 6–9 reveals that the horizontal structure of the histograms (corresponding to constant values of (ϕ_b) is indeed the most relevant variable to measure the shock timing.

The main exception to this rule is shown in Fig. 6(a_1) where the most prominent feature is a diagonal rather than horizontal red region. In this case, the wave front (ϕ_i) is the more relevant quantity in describing the specific DB mechanism. Indeed, the positioning of the wave front close to the anode at the beginning of the shock is a necessary condition for directly blocking the wave propagation.

The most striking feature across all the subplots of Fig. 6 is that the regions of high likelihood of reentrant dynamics removal are strongly localized, only occupying a small percentage of the total area of each plot. This shows that, if we know what ϕ_b and $\Delta\phi$ are when the shock is applied, we can

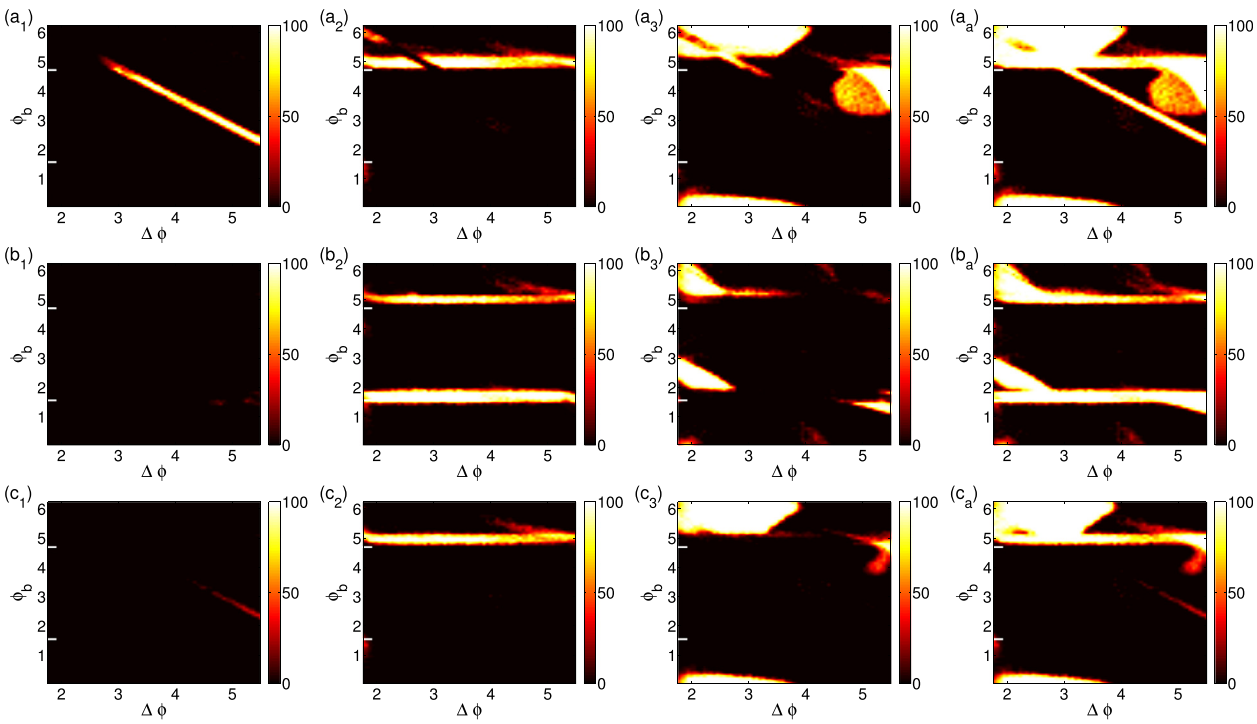

FIG. 6. 2D histograms of the probability of reentrant dynamics removal as a function of the two parameters ϕ_b and $\Delta\phi$ (see text for explanation) for E = 1 V/cm. The top, middle, and bottom rows are for monophasic, biphasic I, and biphasic II, respectively. Subscripts denote different reentrant dynamics removal mechanisms: DB = 1, An = 2, De = 3, and the total for all mechanisms = a. Note that the fourth mechanisms (DA) is not present at low energies and is therefore not shown in this figure.

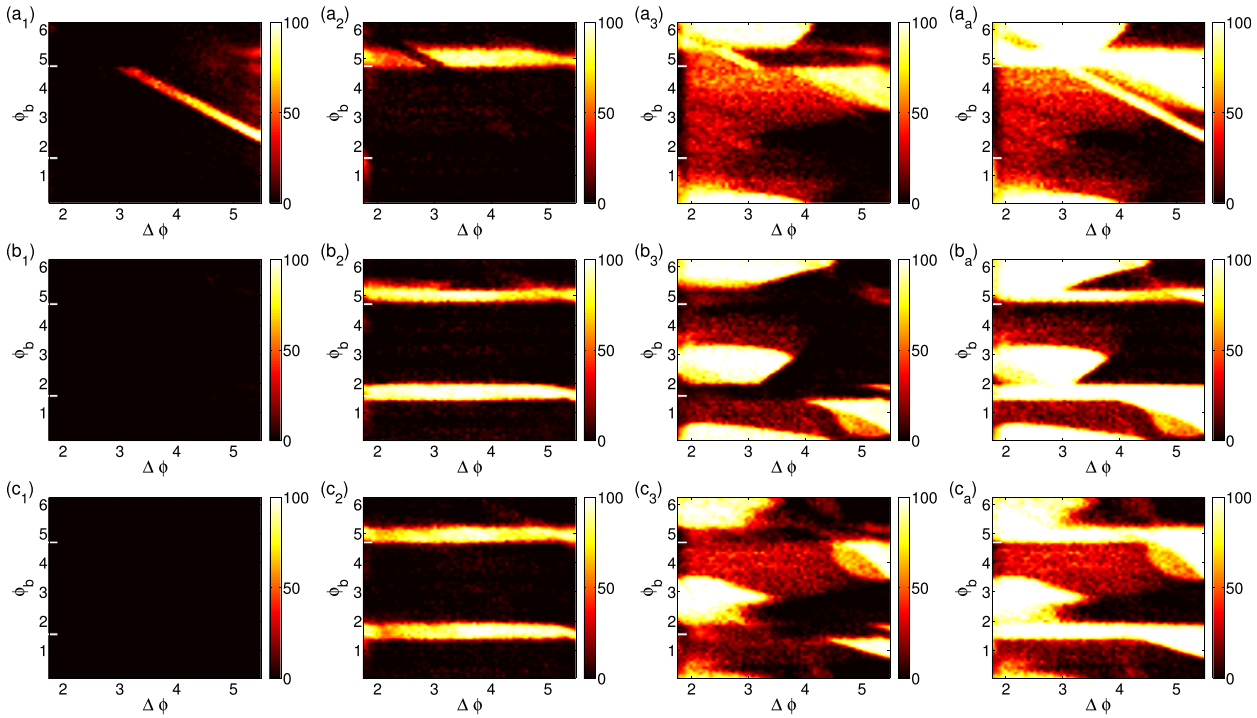

FIG. 7. Same as Fig. 6 for E = 3 V/cm.

predict the outcome with very high precision. The second interesting result from Fig. 6 is the similarity of the subplots of the first and third rows (corresponding to the monophasic and biphasic II protocols, respectively). This indicates that at low energy ($E = 1$ V/cm), the monophasic and biphasic II shocks are the most similar protocols in term of efficiency. The main difference between the first and third rows is the first column (Figs. 6($a1$) and 6($c1$) corresponding to the DB mechanism. The effect of the DB mechanism is only significant for the monophasic protocol.

Figure 7 shows the similar histograms summarizing the results of simulations for $E = 3$ V/cm. Here, the regions of high likelihood of reentrant dynamics removal start to broaden but the outcome is still strongly correlated with particular values of $\Delta\phi$ and ϕ_b. We note that the two biphasic protocols (second and third rows) are now more similar.

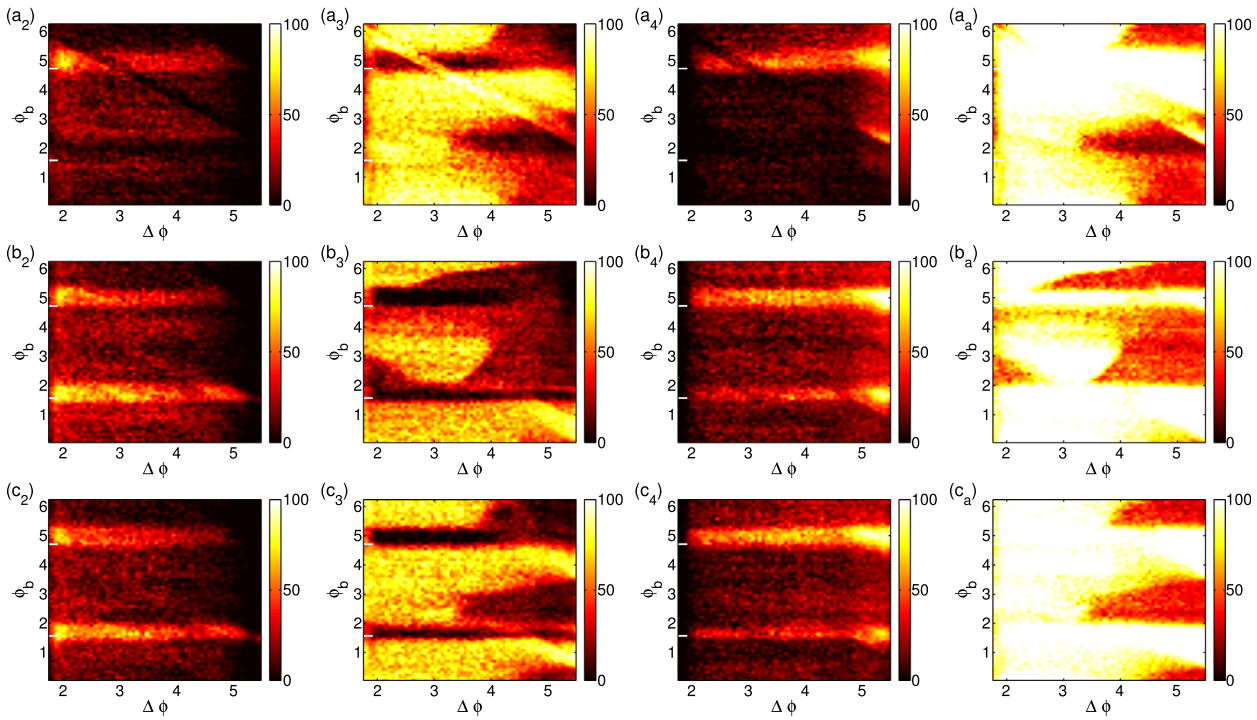

FIG. 8. Same as Fig. 6 for E = 5 V/cm. Note that DB mechanism is not shown here because it is vanishingly small. The histogram for the DA mechanism (subindex = 4) is shown instead.

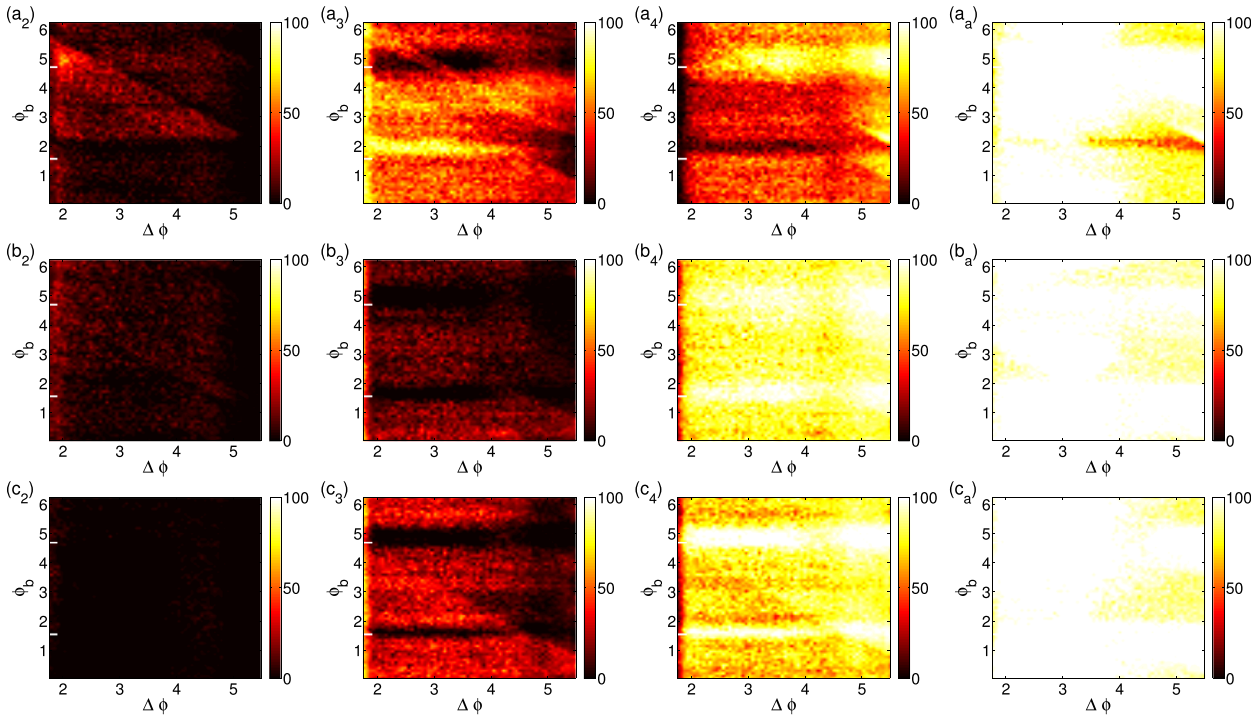

FIG. 9. Same as Fig. 8 for E = 7 V/cm.

One starts to observe regions with intermediate values (i.e., values deviating significantly from 0% or 100% probability of reentrant dynamics removal). The presence of these intermediate values indicate that the two parameters ϕ_b and $\Delta\phi$ are no longer sufficient to determine the outcome of the shock application. Other considerations (e.g., the distribution of the spatial heterogeneities in the conductivity) may also affect the outcome.

In Fig. 8 (which corresponds to $E = 5$ V/cm), we have removed the column for the DB mechanism (subscript 1) and added a column for the DA mechanism (subscript 4). Indeed, at higher energy, the DA mechanism becomes more dominant, while the DB mechanism is not observed. Now, we find that the reentrant dynamics removal probability is considerably higher than for $E = 3$ V/cm. It is also interesting to note that shock works much better for waves with shorter action potential durations. Indeed, low values of $\Delta\phi$ typically correspond to a significantly higher likelihood of defibrillation. This result is not surprising because when $\Delta\phi$ is large, there is very little tissue available to excite, as most of the system is either already excited or is in a refractory state. In contrast, when $\Delta\phi$ is small, a large portion of the tissue is excitable and can be recruited to form virtual electrodes, assisting defibrillation.

From Fig. 9, we see that the DA mechanism is indeed dominant for biphasic shocks at high energy (here $E = 7$ V/cm). Another interesting observation is that for the DA mechanism the regions of high defibrillation probability are rather uniformly spread across the parameter space. This is due to the fact that biphasic shocks render the two electrodes equivalent. On the contrary, for monophasic shocks, one observes in Fig. 9(a_a) that the region with large $\Delta\phi$ where the wave back is located close to the anode ($\phi_b \sim \pi/2$) is not efficiently defibrillated. The reason for this is that this configuration places the wave back at shock initiation close to the hyperpolarized region produced by the anode, rendering the region less refractory. That allows the creation of two waves in the vicinity of the anode. One wave runs into the original wave front, causing the annihilation of both. The other propagates in the same direction as the initial wave and survives. Thus, the shock fails.

We can also use the simulation data to determine the actual time it takes for reentrant dynamics removal to occur. This in turn allows us to identify which of the four reentrant dynamics removal mechanisms is the fastest, and how the time for reentrant dynamics removal is affected by the energy level. These questions can be answered by analyzing the distribution of the time it takes for the last wave front to disappear. The histograms representing this distribution for the three protocols and four different levels of energy, as shown in Fig. 10.

We first note that the last surviving front (when shock is successful) is eliminated well before the end of the simulation (the maximum time of the simulation is 1000 ms). This is a good *a posteriori* check that the integration time we chose was long enough to reliably determine the outcome of the shock.

From Fig. 10, it is obvious that DB and DA are the two fastest mechanisms at low and high energies, respectively. Interestingly, the De mechanism (see Fig 10(a)) has several maxima in the histograms, suggesting more than one subtype of the De mechanism. A closer look at the corresponding simulations show that the surviving front in the De mechanism can persists for as many as two full revolutions around the ring before encountering a refractory region.

Figure 10(a) illustrates once again that many characteristics of the evolution following the shock are similar for

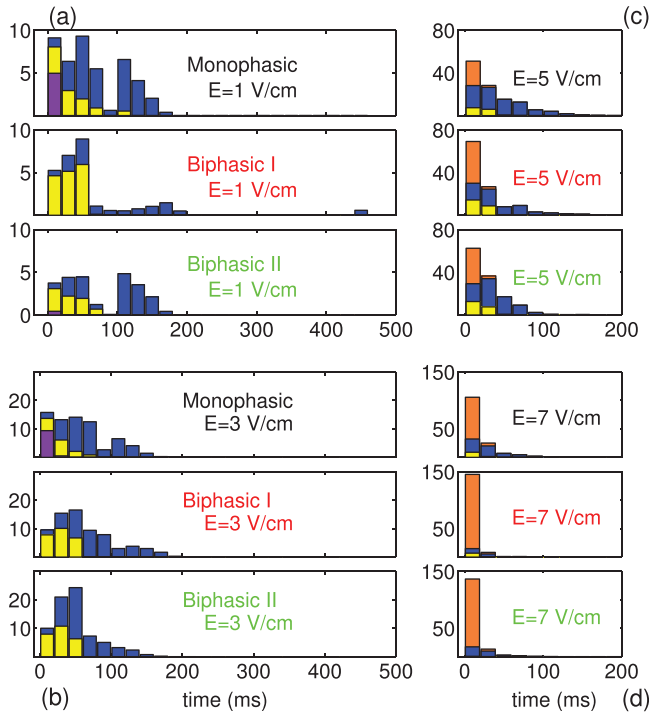

FIG. 10. Histograms showing the time distribution of the disappearance of the last surviving wavefront in the simulations for four shock energy levels (a)–(d), corresponding to $E = 1, 3, 5$, and 7 V/cm, respectively. For each group (a)–(d), the upper, medium and lower sub-graphs indicate monophasic, biphasic I and biphasic II, respectively. The vertical scale of the histogram is in thousands of shock events. The bars all have 20 ms horizontal width. Note that the total number of events for all the subgraphs is the same (160 000). The bar colors indicate the mechanism by which reentrant dynamics removal occurred: DB (purple); An (yellow); De (blue); DA (orange).

monophasic and biphasic II protocols at low energy. In contrast, at high energy (see Fig 10(d)), the dynamics for the two biphasic protocols looks very much alike where the DA mechanism is dominant.

IV. CONCLUSIONS AND FURTHER RESEARCH

In this work, we have developed a one-dimensional numerical model to study reentrant dynamics removal. It should be useful for designing new and more efficient defibrillation protocols because of its simplicity and relatively low computational cost, which allows statistical analysis of large datasets describing tissues with different distributions of heterogeneity. The model is based on a bidomain formulation of cardiac tissue, with the membrane dynamics described by a modified Beeler-Reuter model. We have used the model to compare three standard protocols used in commercial defibrillators—monophasic and two forms of biphasic waveforms. We have performed and analyzed close to five million shock simulations. A careful statistical analysis of the data has allowed us to rank the efficiency of the protocols at high energy tuned to achieve a 90% success rate for a single shock. Biphasic II protocol was determined to be the most efficient, while the monophasic protocol was found to be the least efficient. Specifically, the biphasic II protocol required a shock energy which was 26% less than that required by the monophasic protocol, which is comparable to the available experimental data. The improved efficiency derives from the fact that a larger fraction of the tissue is excited (through the DA mechanism) for the case of biphasic shocks. We have also shown that two parameters, ϕ_b and $\Delta\phi$ describing the shock timing and the system state at the moment of the shock, are important in predicting the outcome of reentrant dynamics removal, especially at lower energies. In the future, we plan to address the question of the influence of another important parameter which is the magnitude of the tissue heterogeneities.

A limitation of our approach is that a 1D model of cardiac activity does not allow for the presence of vortices and rotors, which are very important in the study of arrhythmias. Thus, for example, our model will not be able to reproduce the experimental results that strong shocks sometimes cause fibrillation rather than eliminate it.[14]

We also leave for a future study the question related to the asymmetrical response of the membrane potential with the application of strong electric shocks,[42] which could affect the full generality of our result with respect to the transmembrane model used in the present paper.

Finally, as computational resources continue to improve, we aim to extend our work to two- and three-dimensional tissue to study at a similar level of detail the effects of properties such as multiple reentrant waves, the presence of functional reentries, anisotropy, etc., on defibrillation efficacy and mechanisms.

ACKNOWLEDGMENTS

The financial support from the "Salvador Madariaga" program PR2011-0168 (J.B.) and the research grant FIS2011-28820-C02-02 from the Ministry of Education and Sciences of Spain are acknowledged. A portion of this work (N.F.O., F.H.F., and R.F.G.) was supported by the National Heart, Lung and Blood Institute of the National Institutes of Health, Award No. R01HL089271. This material is also partially based upon work supported by the National Science Foundation under Grant Nos. 1028133 (R.O.G.) and CMMI–1028261 (E.M.C. and F.H.F.). The content is solely the responsibility of the authors, and does not necessarily represent the official views of the NIH.

APPENDIX A: NORMALITY TESTS FOR THE DISPERSION OF THE RESULTS DUE TO THE SPATIAL HETEROGENEITIES

As explained in Sec. III B, the different realizations of the Gaussian noise that are added on top of the intracellular conductivity introduce a dispersion in the results for the defibrillation shocks. Let us recall that each box plot in Fig. 5 condenses the information of 160 000 simulations as follows: 80 realizations of the noise $\times$ 2000 different initial conditions. In order to draw each box plot, we first compute the average probability of defibrillation for the 2000 initial conditions, so that we are left with only 80 data points for drawing the distributions. Usually the distribution of these 80 data points is not compatible with a normal distribution. Table IV confirms that, especially for high energy, a χ^2 test casts some serious doubt on the assumption that the data are

normally distributed. This justifies why, in Sec. III B, we have chosen to use non-parametric testing for ranking the efficiency of the three different defibrillation protocols.

[1]G. Bardy, T. Ivey, M. Allen, G. Johnson, R. Mehra, and H. Greene, "A prospective randomized evaluation of biphasic versus monophasic waveform pulses on defibrillation efficacy in humans," J. Am. Coll. Cardiol. **14**, 728–733 (1989).

[2]R. A. Winkle, R. H. Mead, M. A. Ruder, V. Gaudiani, W. S. Buch, B. Pless, M. Sweeney, and P. Schmidt, "Improved low energy defibrillation efficacy in man with the use of a biphasic truncated exponential waveform," Am. Heart J. **117**, 122–127 (1989).

[3]T. Schneider, P. Martens, H. Paschen, M. Kuisma, B. Wolcke, B. Gliner, J. Russell, W. Weaver, L. Bossaert, and D. Chamberlain, "Multicenter, randomized, controlled trial of 150-J biphasic shocks compared with 200- to 360-J monophasic shocks in the resuscitation of out-of-hospital cardiac arrest victims," Circulation **102**, 1780–1787 (2000).

[4]P. Chen, N. Shibata, E. Dixon, R. Martin, and R. Ideker, "Comparison of the defibrillation threshold and the upper limit of ventricular vulnerability," Circulation **73**, 1022 (1986).

[5]E. Dixon, A. Tang, P. Wolf, J. Meador, M. Fine, R. Calfee, and R. Ideker, "Improved defibrillation thresholds with large contoured epicardial electrodes and biphasic waveforms," Circulation **76**, 1176–1184 (1987).

[6]A. Tang, S. Yabe, J. Wharton, M. Dolker, W. Smith, and R. Ideker, "Ventricular defibrillation using biphasic waveforms: The importance of phasic duration," J. Am. Coll. Cardiol. **13**, 207–214 (1989).

[7]S. Blanchard and R. Ideker, "Mechanisms of electrical defibrillation: Impact of new experimental defibrillator waveforms," Am. Heart J. **127**, 970–977 (1994).

[8]J. Keener and T. Lewis, "The biphasic mystery: Why a biphasic shock is more effective than a monophasic shock for defibrillation," J. Theor. Biol. **200**, 1–17 (1999).

[9]G. W. Beeler and H. Reuter, "Reconstruction of the action potential of ventricular myocardial fibers," J. Physiol. **268**, 177–210 (1977).

[10]K. Skouibine, N. Trayanova, and P. Moore, "A numerically efficient model for simulation of defibrillation in an active bidomain sheet of myocardium," Math. Biosci. **166**, 85–100 (2000).

[11]K. Skouibine, N. Trayanova, and P. Moore, "Success and failure of the defibrillation shock," J. Cardiovasc. Electrophysiol. **11**, 785–796 (2000).

[12]F. Aguel, J. Eason, and N. Trayanova, "Advances in modeling cardiac defibrillation," Int. J. Bifurcation Chaos Appl. Sci. Eng. **13**, 3791–3803 (2003).

[13]N. Trayanova, J. Constantino, T. Ashihara, and G. Plank, "Modeling defibrillation of the heart: Approaches and insights," IEEE Rev. Biomed. Eng. **4**, 89–102 (2011).

[14]I. R. Efimov, Y. Cheng, D. R. Van Wagoner, T. Mazgalev, and P. J. Tchou, "Virtual electrode induced phase singularity: A basic mechanism of defibrillation failure," Circ. Res. **82**, 918–925 (1998).

[15]I. R. Efimov, F. Aguel, Y. Cheng, B. Wollenzier, and N. Trayanova, "Virtual electrode polarization in the far field: implications for external defibrillation," Am. J. Physiol. Heart Circ. Physiol. **279**, H1055–H1070 (2000).

[16]L. Glass and M. E. Josephson, "Resetting and annihilation of reentrant abnormally rapid heartbeat," Phys. Rev. Lett. **75**, 2059 (1995).

[17]P. Comtois and A. Vinet, "Resetting and annihilation of reentrant activity in a model of a one-dimensional loop of ventricular tissue," Chaos **12**, 903–922 (2002).

[18]S. Sinha and D. J. Christini, "Termination of reentry in an inhomogeneous ring of model cardiac cells," Phys. Rev. E **66**, 061903 (2002).

[19]T. Krogh-Madsen and D. J. Christini, "Pacing-induced spatiotemporal dynamics can be exploited to improve reentry termination efficacy," Phys. Rev. E **80**, 021924 (2009).

[20]N. F. Otani, "Termination of reentrant cardiac action potential propagation using far-field electrical pacing," IEEE Trans. Biomed. Eng. **58**, 2013–2022 (2011).

[21]F. H. Fenton, S. Luther, E. M. Cherry, N. F. Otani, V. Krinsky, A. Pumir, E. Bodenschatz, and R. F. Gilmour, "Termination of atrial fibrillation using pulsed low-energy far-field stimulation," Circulation **120**, 467–476 (2009).

[22]S. Luther, F. H. Fenton, B. G. Kornreich, A. Squires, P. Bittihn, D. Hornung, M. Zabel, J. Flanders, A. Gladuli, L. Campoy, E. M. Cherry, G. Luther, G. Hasenfuss, V. I. Krinsky, A. Pumir, R. F. Gilmour, and E. Bodenschatz, "Low-energy control of electrical turbulence in the heart," Nature **475**, 235–239 (2011).

[23]M. Courtemanche, "Complex spiral wave dynamics in a spatially distributed ionic model of cardiac electrical activity," Chaos **6**(4), 579–600 (1996).

[24]J. Keener and J. Sneyd, *Mathematical Physiology* (Springer, 1998).

[25]K. Debruin and W. Krassowska, "Electroporation and shock-induced transmembrane potential in a cardiac fiber during defibrillation strength shocks," Ann. Biomed. Eng. **26**, 584–596 (1998).

[26]R. Ranjan, N. Chiamvimonvat, N. Thakor, G. Tomaselli, and E. Marban, "Mechanism of anode break stimulation in the heart," Biophys. J. **74**, 1850–1863 (1998).

[27]Y. Saad and M. H. Schultz, "Gmres—a generalized minimal residual algorithm for solving nonsymmetric linear-systems," SIAM J. Sci. Comput. (USA) **7**, 856–869 (1986).

[28]S. Balay, J. Brown, K. Buschelman, W. D. Gropp, D. Kaushik, M. G. Knepley, L. C. McInnes, B. F. Smith, and H. Zhang, see http://www.mcs.anl.gov/petsc for PETSc Web page (2012).

[29]M. G. Fishler, E. A. Sobie, L. Tung, and N. V. Thakor, "Cardiac responses to premature monophasic and biphasic field stimuli. Results from cell and tissue modeling studies," J. Electrocardiol. **28**(Suppl), 174–179 (1995).

[30]G. Plank, L. Leon, S. Kimber, and E. Vigmond, "Defibrillation depends on conductivity fluctuations and the degree of disorganization in reentry patterns," J. Cardiovasc. Electrophysiol. **16**, 205–216 (2005).

[31]M. Courtemanche, L. Glass, and J. P. Keener, "Instabilities of a propagating pulse in a ring of excitable media," Phys. Rev. Lett. **70**, 2182 (1993).

[32]M. A. Watanabe, F. H. Fenton, S. J. Evans, H. M. Hastings, and A. Karma, "Mechanisms for discordant alternans," J. Cardiovasc. Electrophysiol. **12**, 196–206 (2001).

[33]J. M. Pastore, S. D. Girouard, K. R. Laurita, F. G. Akar, and D. S. Rosenbaum, "Mechanism linking T-wave alternans to the genesis of cardiac fibrillation," Circulation **99**, 1385–1394 (1999).

[34]R. X. Stroobandt, S. Barold, and A. Sinnaeve, *Implantable Cardioverter-Defibrillators Step by Step* (Wiley-Blackwell, 2009).

[35]Z. Qu, J. Weiss, and A. Garfinkel, "Spatiotemporal chaos in a simulated ring of cardiac cells," Phys. Rev. Lett. **78**(7), 1387 (1997).

[36]C. Bishop, *Neural Networks for Pattern Recognition* (Oxford University Press, 1995).

[37]MATLAB, *version* 7.9.0 (R2009b) (The MathWorks Inc., Natick, Massachusetts, 2009).

[38]M. Li and N. Otani, "Controlling alternans in cardiac cells," Ann. Biomed. Eng. **32**, 784–792 (2004).

[39]D. Allexandre and N. Otani, "Preventing alternans-induced spiral wave breakup in cardiac tissue: An ion-channel-based approach," Phys. Rev. E **70**, 061903 (2004).

[40]A. Garzon, R. O. Grigoriev, and F. H. Fenton, "Model-based control of cardiac alternans on a ring," Phys. Rev. E **80**, 021932 (2009).

[41]A. Garzon, R. O. Grigoriev, and F. H. Fenton, "Model-based control of cardiac alternans in Purkinje fibers," Phys. Rev. E **84**, 041927 (2011).

[42]T. Ashihara and N. A. Trayanova, "Asymmetry in membrane responses to electric shocks: Insights from bidomain simulations," Biophys. J. **87**, 2271–2282 (2004).